

Automatic localization of anatomical landmarks in 2D MRI localizer sequence using deep convolutional neural network

By

DIVYA SHAH
(202111040)

A Thesis Submitted in Partial Fulfilment of the Requirements for the Degree of

MASTER OF TECHNOLOGY
in
INFORMATION AND COMMUNICATION TECHNOLOGY
to

DHIRUBHAI AMBANI INSTITUTE OF INFORMATION AND COMMUNICATION TECHNOLOGY

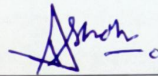


May, 2023

Declaration

I hereby declare that

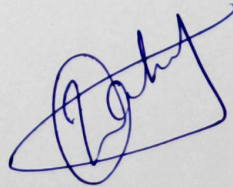
- i) the thesis comprises of my original work towards the degree of Master of Technology in Information and Communication Technology at DA-IICT and has not been submitted elsewhere for a degree,
- ii) due acknowledgement has been made in the text to all the reference material used.



Divya Shah

Certificate

This is to certify that the thesis work entitled "**Automatic localization of anatomical Landmarks in 2D MRI localizer sequence using Deep Convolutional Neural Network**" has been carried out by **Divya Shah (202111040)** for the degree of Master of Technology in Information and Communication Technology at Dhirubhai Ambani Institute of Information and Communication Technology under my supervision.



Prof. Bakul Gohel

Acknowledgement

I want to extend sincere gratitude to my thesis supervisor, **Prof. Bakul Gohel**, who has been an exceptional mentor throughout my research work. Prof. Gohel's exceptional expertise as a medical professional has been instrumental in deepening my understanding of the medical aspects of my thesis study. His insights and extensive knowledge in the field have provided crucial perspectives that have significantly influenced the development of my ideas. I am genuinely grateful for his unwavering support and continuous encouragement throughout this journey.

Secondly, I sincerely thank Lalit Kumar for his valuable contributions to this research project. Lalit played a crucial role in the initial stages of the study, assisting in conducting the pilot study. His dedication and efforts have been instrumental in laying the foundation for this work. I appreciate his support, insights, and collaborative spirit, which have helped make this a successful research endeavor.

Further, I also extend heartfelt thanks to my friends who always stood beside me and motivated me throughout the journey of this thesis work. A few include Nisarg, Hemani, Krutika, Ruchita, Shreyas, Dhairya, Abhishek, and Juned. Finally, I sincerely thank Mom and Dad for their constant support throughout the M.Tech journey. With them, it was possible to complete my thesis work. Their blessings have guided me throughout this journey.

Contents

Abstract	v
List of Acronyms	vi
List of Tables	vii
List of Figures	viii
1 Introduction	1
1.1 Problem Statement and Motivation.....	2
1.1.1 Problem Statement	2
1.1.2 Motivation.....	2
1.2 Contributions	2
1.3 Organization of Thesis.....	3
2 Fundamentals	4
2.1 MRI Scan Acquisition	4
2.1.1 Basic Principle	4
2.1.2 Components of MRI Machine	5
2.1.3 MRI Slice Selection	6
2.2 Importance of MRI Orientation.....	7
2.3 MRI Localizer Scan (Scout Scan).....	7
2.4 K-Space	9
2.5 Chapter Summary	9
3 Related Work	10
3.1 Detection in the 2D Slices	10
3.2 Detection in the 3D MRI Volume.....	12
3.3 Other Methodologies	12
3.4 Chapter Summary	13
4 Methodology	14
4.1 Network Architecture	14
4.2 Dataset.....	17
4.3 Data Pre-processing	18
4.4 Loss Function	19
4.5 Chapter Summary	19

5 Experiment and Results	21
5.1 Training.....	21
5.1.1 Low Pass Filtering	22
5.2 Unit Testing	24
5.3 Testing Workflow	26
5.4 Outcomes.....	27
5.5 Chapter Summary	28
6 Discussion and Conclusion	29
6.1 Discussion.....	29
6.2 Conclusion.....	30
6.3 Future Work.....	30
References	31

Abstract

In Medical Imaging of the brain, especially Magnetic Resonance Imaging (MRI), localizing various anatomical landmarks like the Anterior and Posterior Commissure (A.C./P.C.) and Mid-Sagittal plane (MSP) is crucial for good quality MRI. By convention, during brain MRI scan acquisition, the radiographer first performs a three-plane MRI localizer slice acquisition protocol to obtain these landmarks. This process is called Scout Scan. However, this is a tedious job and is susceptible to operator error. Also, the MRI scan's resolution is anisotropic, i.e., good in-plane and lower out-of-plane resolution. As a result, a change in head position might significantly impact the interpretation of an MRI \ image. Hence, Automizing this process is vital to reduce operator error.

Previous works predict A.C. and P.C. points in the Mid-sagittal plane, but the improper head position may lead to an improper Mid-sagittal plane (MSP). Hence, it may lead to localization errors. Also, previous works predict this point in a 3D voxel, which is impractical. To obtain a 3D voxel, longer time and computational resources are required. Furthermore, G.E.'s healthcare system has developed a similar tool named "AIRx, but it takes 9 to 20 Localizer slices to predict these landmarks.

This work presents the deep learning-based automated localizing of these landmarks in 3D space for the brain from a three-plane 2D MRI localizer slice. This work uses six publicly available brain MRI datasets and a few image augmentation techniques. The mean error in localization of A.C. and P.C. within the dataset is less than 1mm. For cross dataset, it is less than 2mm, and also mean error in degrees for finding orientation vector is less than 2° for both within and cross dataset.

List of Acronyms

MRI	Magnetic resonance imaging
CNN	Convolutional Neural Network
A.C.	Anterior Commissure
P.C.	Posterior Commissure
RF	Radio Frequency
ReLu	Rectified Linear unit
DOF	Degrees of Freedom
MSE	Mean Square Error
R-CNN	Region-based Convolutional Neural Network
ABA	Adaptive Bases Algorithm
MBJ	Mid-brain Pons Junction

List of Tables

Table 4.1 Architecture Details.....	16
Table 4.2 Dataset Details	18
Table 5.1 $\pm 20\text{mm}$ Translation and 30° Rotation	25
Table 5.2 $\pm 5\text{mm}$ Translation and 15° Rotation	25
Table 5.3 Within Dataset.....	27
Table 5.4 Cross Dataset.....	27

List of Figures

Figure 2.1 Different Orientation of Image Acquisition	6
Figure 2.2 A.C. and P.C. Landmarks	8
Figure 2.3 The MSP represented as the vertical dashed-yellow axis.....	8
Figure 3.1 Point Detection Model	10
Figure 3.2 Angle Detection Model.....	11
Figure 3.3 Multi-task Model	11
Figure 4.1 Custom CNN architecture	15
Figure 4.2 Homogeneous Ensemble Model	17
Figure 4.3 Pre-processing of Dataset.....	19
Figure 5.1 Low Pass Filtering using Fourier transformation.....	22
Figure 5.2 Original Image	23
Figure 5.3 25% Low-filtered Image.....	23
Figure 5.4 5% Low-filtered Image.....	24
Figure 5.5 1% Low-filtered Image.....	24
Figure 5.6 Testing Pipeline.....	26

CHAPTER 1

Introduction

Consistent and uniform placement of the MR slices during MR neuroimaging is critical for performing inter- and intra-scan comparisons. MRI resolution is often anisotropic, i.e., a good “in-plane” resolution and a reduced “out-of-plane” resolution are frequently found in MRI scans with varying resolutions and orientations[1]. The difference in the subject’s positioning is unavoidable. If this deviation is more prominent from the desired head orientation, it may cause severe difficulties in interpreting the image obtained from MRI[2]. For example, Reuter et al.,2014 demonstrated in their work that the differences in head position might significantly impact tumor region area measurements[1], [3]. Hence, for accurate positioning of the brain MRI, identification of anatomical landmarks such as anterior commissure (A.C.), posterior commissure (P.C.), and mid-sagittal plane (MSP) are necessary[2].

Consequently, before conducting a full MRI scan, a three-plane localizer MR scan (also known as a scout scan) is typically performed by radiographers to identify specific landmarks in the sagittal, coronal, or horizontal planes[4], [5]. This process has often been done manually, which is time-consuming and error-prone because of inter-operator variability. To address this issue, automating the MR slice orientation and positioning process could help reduce operator inconsistency, enhance accuracy, and potentially reduce the overall duration of the scan.

The A.C., P.C., and MSP are significant landmarks that help to characterize the brain's anatomical coordinates[6]–[8]. Further, these landmarks have substantial applications in various neuro-surgical procedures such as deep brain stimulation[9], image registration [10], and human brain mapping [11]. Many model-based techniques have been published priorly to automate the detection of these anatomical landmarks, where A.C. and P.C. locations were identified using template matching[12]–[14]. Recently, Yuan Liu and Benoit Dawant have used Regression Forest to automate A.C., P.C., and MSP localization in MRI scans[15]. Deep learning algorithms have recently gained popularity in various medical image analytics [16]–[18]. Many deep learning-based algorithms have also been used to detect A.C. and P.C. anatomical landmark detection in the 2D scan [1], [19] or 3D MRI Volume[15], [20]. In a three-plane MRI localizer (scout) scan, we have three 2D brain MRI slices. The goal is to localize A.C. and P.C. in a mid-sagittal brain MRI slice and to make an angle prediction.

1.1 Problem Statement and Motivation

1.1.1 Problem Statement

In previous works, the prediction of the A.C. and P.C. points has primarily focused on the mid-sagittal plane[1], [19]. However, a significant limitation of this approach arises from the potential for improper head positioning, which can result in an inaccurate mid-sagittal plane (MSP) estimation. Consequently, A.C. and P.C. landmarks localization may be prone to errors.

Moreover, previous methodologies often rely on predicting these landmarks in a 3D voxel [15]. However, this is not feasible, as it necessitates a significant amount of time to procure a complete 3D voxel image. This time-consuming process can impede the efficiency of the localization task and limit its clinical applicability.

It is worth noting that G.E.'s healthcare system has developed a similar tool known as "AIRx"[21], which also aims to predict A.C. and P.C. landmarks. However, this tool requires the utilization of 9 to 20 localizer slices for accurate prediction. This substantial number of slices further adds to the complexity and resource requirements of the process.

1.1.2 Motivation

Considering these limitations in the existing approaches, there is a need to develop a more robust and efficient methodology for predicting A.C. and P.C. points. This methodology should address the challenges associated with improper head positioning, the practicality of 3D voxel-based prediction, and the resource-intensive nature of current tools such as "AIRx." By addressing these issues, the proposed methodology aims to enhance the accuracy, efficiency, and clinical utility of A.C. and P.C. localization in neuroimaging applications. Deep convolution neural networks are used in the current study to predict A.C. and P.C. landmarks in 3D space directly from a three-plane MRI localizer slice. Deep learning applications for medical imaging have significant difficulties with data variability and repeatability [22], [23]. Deep learning-based methodologies are also susceptible to data bias [24], [25].

Therefore, this work aims to directly predict the A.C., P.C., and Orientation vector in the 3D space from three-plane 2D MRI Localizer slices using Deep Convolutional Neural Network. Further, we evaluated our model with a cross-dataset to analyze its generalization capabilities and resolve the issue of data bias.

1.2 Contributions

Our work contributes to the field of MRI neuroimaging by introducing a robust methodology for automated landmark localization using a deep convolutional neural network. The proposed approach enhances the accuracy of anterior and posterior commissure (A.C. and P.C.) landmark prediction by considering potential head

positioning deviations. Further, this methodology directly predicts A.C. and P.C. landmarks in 3D space from three-plane 2D MRI localizer slices, hence addressing the challenge of computational complexity and enhancing the practicality and applicability of automated landmark localization in a real-world application. Furthermore, the cross-dataset evaluation ensures the method's generalization capabilities and minimizes data bias, reinforcing its reliability in diverse clinical settings. Ultimately, these contributions advance neuroimaging analyses, offering a practical and impactful solution for improved patient care and clinical decision-making by improving efficiency without compromising accuracy.

1.3 Organization of Thesis

Six chapters make up the structure of this thesis as below:

Chapter 2: "Fundamentals" deals with the fundamental concepts and theoretical foundations crucial for this study.

Chapter 3: "Literature Survey," presents a comprehensive review of relevant literature and studies on A.C. and P.C. localization in neuroimaging. This chapter explores previous research works, methodologies, and advancements in the field.

Chapter 4: "Methodology," shows the proposed methodology for A.C., P.C., and Orientation Vector prediction in detail.

Chapter 5: "Implementation," focuses on the practical aspects of implementing the proposed methodology.

Finally, **Chapter 6:** "Discussion and Conclusion," provides a comprehensive analysis and interpretation of the results obtained from the implementation.

CHAPTER 2

Fundamentals

This chapter delves into the fundamental concepts and theoretical foundations that form the basis of the research. This chapter provides an in-depth discussion of key topics such as "MRI Scan Acquisition", "Importance of MRI Orientation", "Scout Scan", and "K-Space". Understanding these fundamental concepts is crucial for comprehending the subsequent chapters and the proposed methodology.

2.1 MRI Scan Acquisition

In this section, we have explained the basic principles of MRI scan acquisition.

2.1.1 Basic Principle

MRI is a medical imaging method used in radiology to see the human body's physiology, including its anatomy, in both health and disease. MRI acquisition is based on the magnetic properties of certain atomic nuclei, particularly the hydrogen nucleus (proton). When a patient is placed in the powerful magnetic field of an MRI scanner, the hydrogen nuclei align themselves partially with the magnetic field, akin to a magnetic compass[26].

To manipulate these aligned nuclei and generate a measurable signal, radio waves emitted by the MRI scanner are used. The radio waves have a specific frequency corresponding to the hydrogen nuclei's Larmor frequency. The aligned hydrogen nuclei can be rotated or "flipped" by applying radio waves at the appropriate frequency and orientation[27].

Once the radio wave is turned off, the hydrogen nuclei return to their equilibrium state and emit radio signals in the form of electromagnetic radiation. These emitted signals are picked up by antennas or receiver coils surrounding the patient. The strength and timing of these radio signals provide information about the local tissue characteristics.

The acquired radio signals contain valuable data about the spatial distribution of the hydrogen nuclei and their magnetic properties. However, the signals are initially represented in a mathematical space called "k-space." K-space is a matrix-like representation where each point corresponds to a specific frequency and phase. A mathematical process called the Fourier transform is applied to convert the data from k-space into a visual representation of the anatomical structures to obtain the final image[28].

2.1.2 Components of MRI Machine

The MRI machine consists of four major components, each playing a crucial role in imaging. These components are the Main Magnet, Gradient Coils, Radio Frequency Transmitter/Receiver Coils, and the Computer System. The following is an expanded description of each component, highlighting their significance and functions within the MRI system.

1. **Main Magnet:**

The Main Magnet is a fundamental component of the MRI machine, formed by superconducting coils. These coils generate a strong, uniform magnetic field that is essential for the functioning of MRI. The magnetic field strength is typically measured in Tesla (T) and can range from 1.5T to 7T in modern MRI systems. The Main Magnet provides the magnetic field to align the hydrogen nuclei within the patient's body, facilitating the subsequent imaging process[26].

2. **Gradient Coils:**

Gradient Coils are a set of smaller, specialized coils positioned within the Main Magnet. These coils produce controlled variations in the magnetic field strength along different spatial directions, typically the x, y, and z axes. By varying the strength and timing of these magnetic field gradients, the Gradient Coils enable spatial encoding, allowing precise localization of signals emitted by the hydrogen nuclei. This spatial information is crucial for generating detailed images and differentiating structures within the imaged area[27].

3. **Radio Frequency Transmitter/Receiver Coils:**

The Radio Frequency (RF) Transmitter/Receiver Coils serve as the interface between the MRI machine and the patient. The RF Transmitter coil emits radio waves at a specific frequency and orientation, targeting the hydrogen nuclei within the imaged region. These radio waves manipulate the hydrogen nuclei effectively, altering their alignment and generating a detectable signal. The RF Receiver coil, positioned around the patient, captures the emitted radio signals and transmits them for processing and image reconstruction to computer systems[26].

4. **Computer System:**

The Computer System is the central component that controls the MRI machine's operation, acquisition parameters, and data processing. It coordinates the interplay of the Main Magnet, Gradient Coils, and RF Coils to generate high-quality MRI images. The computer system also performs complex mathematical operations, such as Fourier transform and image reconstruction, to convert the acquired raw data into visual representations of the anatomical structures. Furthermore, the computer system provides a user interface for the operator to interact with the MRI machine, set imaging parameters, and monitor the scanning process[26].

2.1.3 MRI Slice Selection

One crucial step in MRI scan acquisition is Slice Selection, which determines the orientation of the slice to be acquired. MRI can acquire images in any desired orientation, allowing flexibility in examining various anatomical structures.

To achieve slice selection, a frequency-selective RF pulse is utilized in conjunction with one of the magnetic field gradients, namely G_x , G_y , or G_z (Figure 2.1). These gradients are responsible for spatial encoding and determining the slice location within the imaging volume[27].

During the slice selection process, the frequency-selective RF pulse is applied in the presence of the desired gradient, which corresponds to the desired slice orientation. The RF pulse is designed to selectively excite the spins within the chosen slice while suppressing the signals from other slices. This selective excitation is achieved by adjusting the RF pulse's frequency and timing parameters to match the spins' resonant frequency within the targeted slice.

Upon excitation, the spins within the selected slice enter a transient high-energy state and start to precess. Subsequently, the MRI system measures the resulting signals emitted by these excited spins using the receiver coils. The acquired signal data contains spatial and frequency information specific to the selected slice.

Slice selection, along with other pulse sequences and imaging parameters, plays a crucial role in obtaining high-quality MRI images. It allows for the precise localization of the imaging slice within the three-dimensional anatomical space, enabling detailed examination of specific regions of interest.

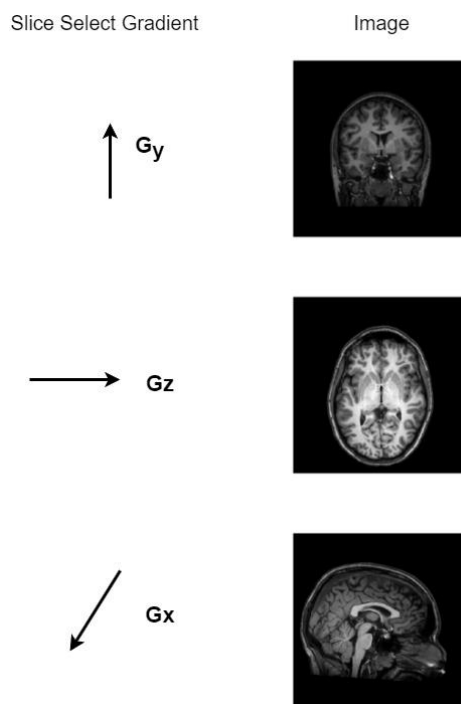


Figure 2.1 Different Orientation of Image Acquisition

2.2 Importance of MRI Orientation

MRI image resolution exhibits an anisotropic nature. This implies that there is a variation in resolution along different spatial dimensions. MRI tends to have good "in-plane" resolution while lower "out-plane" resolution[1].

The variation in resolution can occur due to unavoidable differences in subject positioning during MRI scans. MRI images are typically reviewed as 2D slices. Any alterations in head orientation can significantly impact the accurate interpretation of these images. If this deviation is prominent, then it may severely pose a challenge in interpreting these images[2]. Hence, it is crucial to ensure that observed brain asymmetry is attributed to pathological conditions rather than variations in head positioning or the prescribed scanning configuration.

Therefore, it is essential to recognize the head position and ensure proper alignment during the MRI scan. Establishing the correct location and orientation of an MRI slice for a whole-brain MRI scan is particularly important. This ensures that the acquired slices cover the entire brain region of interest and are aligned in a standardized manner.

By acknowledging the importance of MRI orientation and ensuring proper alignment, clinical practitioners can improve the accuracy and reliability of their interpretations. This understanding contributes to effectively utilizing MRI images for diagnostic and research purposes.

2.3 MRI Localizer Scan (Scout Scan)

An MRI Scout Scan, also known as a localizer or survey scan, is an initial imaging sequence performed before the actual MRI examination. Its purpose is to provide an overview or scout image of the patient's anatomy, helping to guide the subsequent acquisition of specific imaging planes or sequences.

During the MRI Scout Scan, the radiographer or technician acquires images in different orientations (sagittal, coronal, and axial) to visualize the anatomical landmarks and determine the patient's positioning within the MRI scanner. These localizer slices are in low resolution. Amongst the anatomical landmarks, Anterior Commissure (A.C.), Posterior Commissure (P.C.), (Figure 2.2) and Mid-sagittal Plane (MSP) (Figure 2.3) are the most significant. These images serve as reference images for accurately planning and positioning the subsequent MRI sequences.

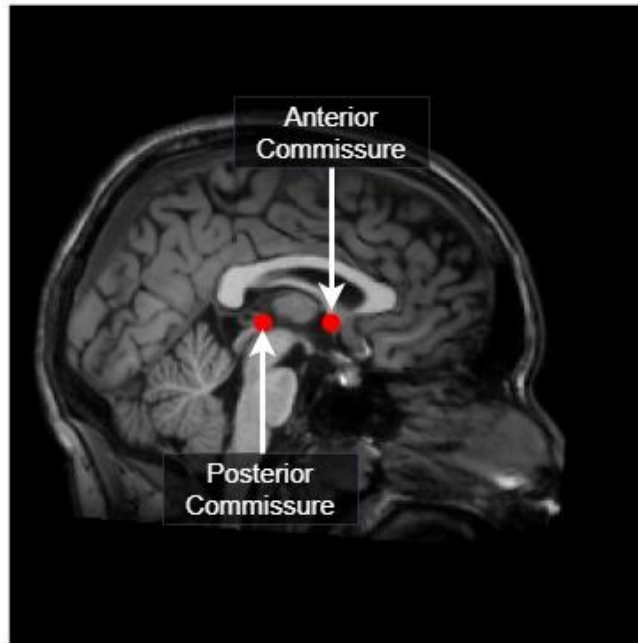


Figure 2.2 A.C. and P.C. Landmarks

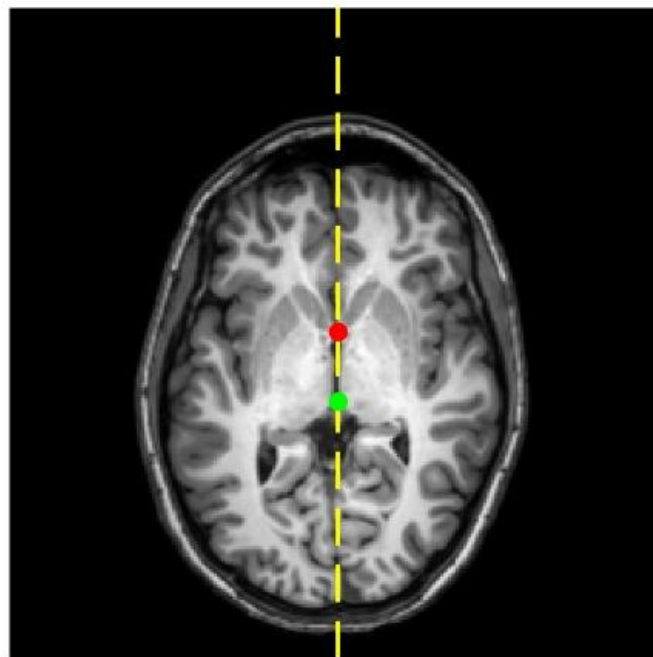


Figure 2.3 The MSP represented as the vertical dashed-yellow axis

The Scout Scan allows the radiographer to identify essential structures, such as the brain, spinal cord, or specific regions of interest. It ensures that the subsequent imaging planes are adequately aligned. By visually inspecting the Scout Scan images, the radiographer can verify the coverage of the desired anatomy and make any necessary adjustments before proceeding with the actual diagnostic MRI sequences.

The Scout Scan also aids in reducing the chances of missing relevant anatomical regions and helps to minimize imaging artifacts that could interfere with the interpretation of the diagnostic images. It provides essential information for

optimizing the image acquisition process and improving the overall quality of the MRI examination.

2.4 K-Space

In MRI, k-space represents the spatial frequency content of the MR image. It can be visualized as a rectangular grid with principal axes kx and ky , which correspond to spatial frequencies in the x and y directions, respectively. The arrangement of cells in k-space reflects the distribution of different spatial frequencies within the MR image.

In k-space, higher frequencies are located toward the outer edges of the grid, while lower frequencies are closer to the center. This means that the cells near the center of the k-space represent the low-frequency components of the image, which contribute to the overall structural information. The cells farther from the center represent higher-frequency components, contributing to finer details and sharper features in the image.

The relationship between the MR image and k-space is based on the Fourier Transform. The Fourier Transform mathematically converts an image from the spatial domain to the frequency domain. In the context of MRI, the MR image is gained by applying the inverse Fourier Transform to the data in k-space. This conversion reconstructs the image by assigning appropriate intensities to the corresponding spatial locations.

By performing the inverse Fourier Transform on the k-space data, the spatial frequencies are transformed back into the spatial domain, resulting in the MR image as we perceive it. This process assigns intensity values to each pixel, creating a representation of the anatomical structures and features present in the original image.

2.5 Chapter Summary

This chapter thoroughly comprehends the fundamental principles underlying MRI scan acquisition. It begins by explaining the basic principle of MRI, which relies on the magnetic properties of hydrogen nuclei in the presence of a strong magnetic field and how it is aligned in the presence of radio waves. Additionally, it discusses the concept of k-space, a mathematical representation of acquired data, and the application of the Fourier transform to convert this data into visual representations. The chapter further explores the components of an MRI machine, including the main magnet, gradient coils, radio frequency transmitter/receiver coils, and the computer system, highlighting their roles in the imaging process. Finally, it delves into the importance of MRI orientation, the significance of MRI localizer scans, and the utilization of k-space in image reconstruction.

CHAPTER 3

Related Work

This chapter showcases the relevant literature and studies on A.C. and P.C. localization in neuroimaging. It explores previous research works, methodologies, and advancements in the field. It critically evaluates the strengths and weaknesses of existing approaches and identifies research gaps that the current study aims to address.

3.1 Detection in the 2D Slices

Recently, Xulei Yang et al. proposed a method for automatically detecting anatomical landmarks in brain M.R. scans. The method uses a multi-task deep neural network (Figure 3.3) trained to detect the anterior commissure (A.C.), posterior commissure (P.C.), and symmetry lines in the sagittal and axial images simultaneously. The multi-task learning architecture improves learning efficiency and prediction efficiency by exploiting the similarities and differences across the tasks (Figure 3.1 and Figure 3.2). Following the derivation of the A.C. – P.C. line and symmetry line on the sagittal and axial images, the corresponding scan coverage is estimated using an image processing technique. The main disadvantage of this work is that the radiologist may not be able to procure a proper mid-sagittal slice while performing the MRI localizing sequence due to improper head position. As a result, the A.C. and P.C. landmark positions in that 2D slice and their positions in 3D space may not be perfect[1].

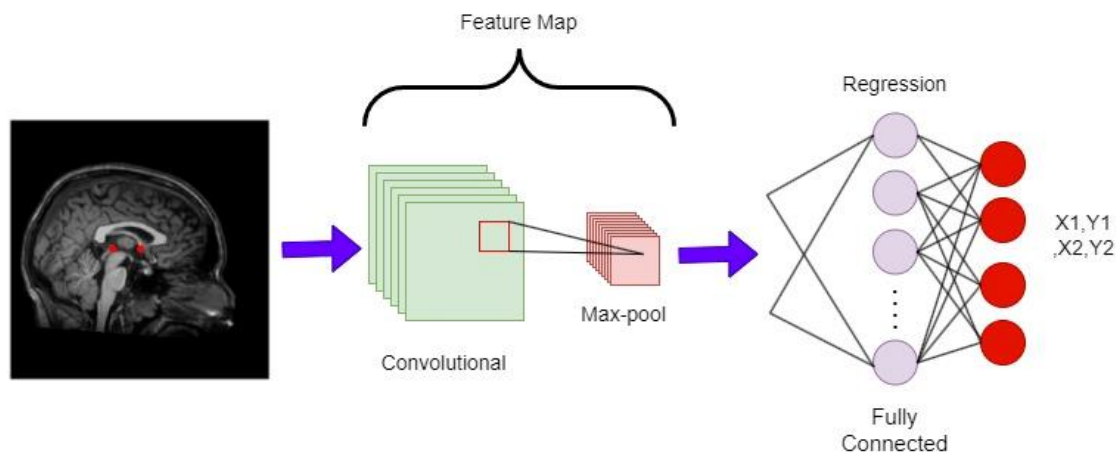


Figure 3.1 Point Detection Model

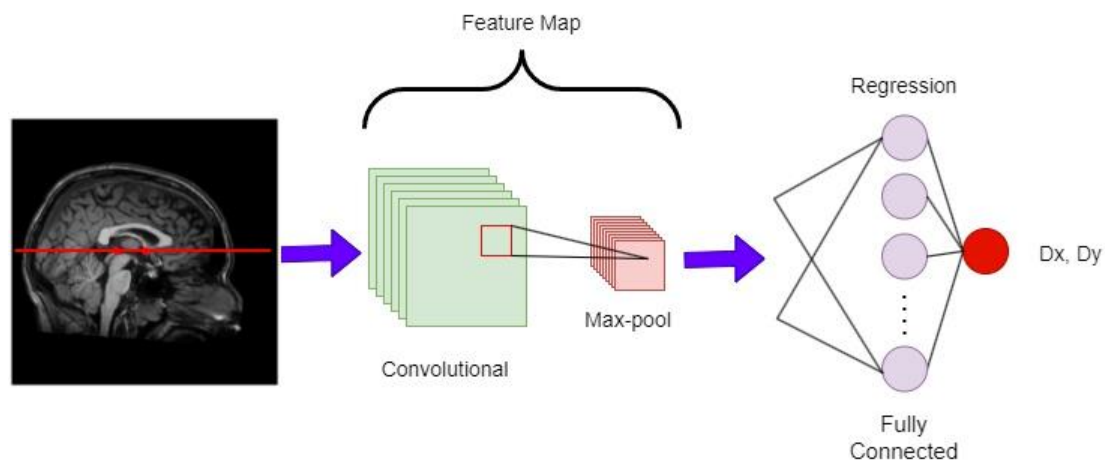


Figure 3.2 Angle Detection Model

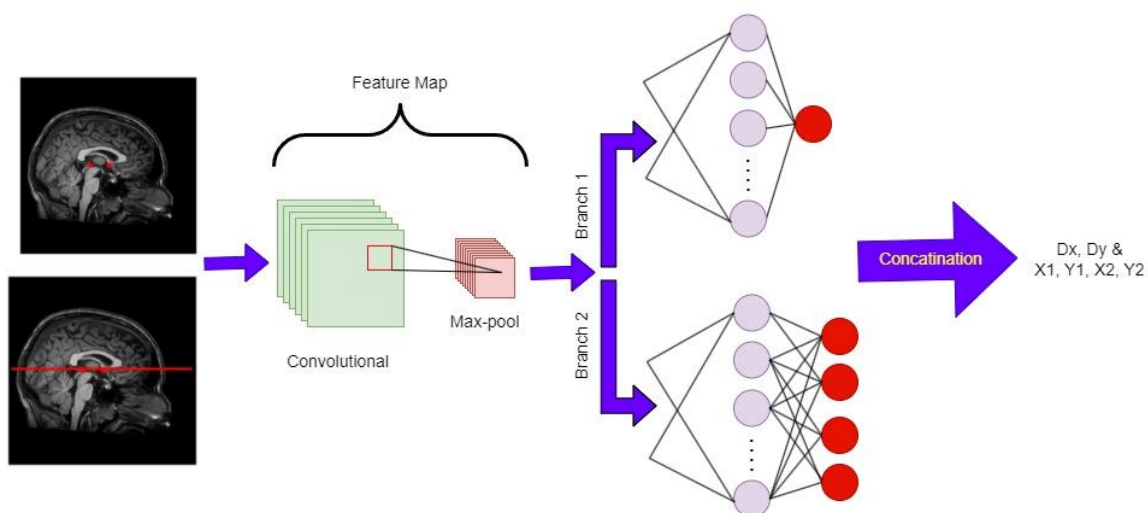


Figure 3.3 Multi-task Model

Hiroyuki Sugimori and Masashi Kawakami's work proposes a method for automatically detecting a standard line in brain magnetic resonance imaging (MRI) scans. The proposed methodology utilizes an advanced deep learning algorithm known as Faster R-CNN (Region-based Convolutional Neural Network) to identify the orbitomeatal line (OM-line), a commonly used reference line for aligning brain MRI scans. The effectiveness of this approach was evaluated on a comprehensive dataset comprising 1200 brain MRI scans, and the results demonstrated a satisfactory level of accuracy in OM-line detection[19].

3.2 Detection in the 3D MRI Volume

In the work of Yuan Liu and Benoit Dawant, they have proposed a learning-based method for automatic and efficient detection of A.C., P.C., and MSP using regression forest. They used random forest models to understand the nonlinear relation between the attributes taken from a point in an image and the likelihood or probability that the point is a landmark. Three-stage coarse-to-fine models are trained individually for the A.C., P.C., and MSP using downsampled by 4, downsampled by 2, and the original pictures. Localization is performed hierarchically, beginning with a preliminary estimate and gradually refining it[15].

Recently, Christine A. Edwards et al. proposes a deep learning-based method for automatically localizing the anterior commissure (A.C.) and posterior commissure (P.C.) in magnetic resonance imaging (MRI) scans. The proposed method, DeepNavNet, is a convolutional neural network that is trained to regress the 3D coordinates of the A.C. and P.C. from MRI scans. DeepNavNet was trained on a dataset of 1128 publicly available MRI scans and was evaluated on a test dataset of 311 MRI scans[20].

3.3 Other Methodologies

In the work of B. A. Ardekani and A. H. Bachman, they have presented an automatic model-based approach to detect A.C. and P.C. on the brain's MRI scan. In the study, they have initially located these landmarks manually with the help of experts, which were then used to detect A.C. and P.C. landmarks on the test scan. The authors have claimed this method to be robust against different contrasts and scanning modes, and it is also optimized against different populations. The algorithm used does not rely on the localization of the Corpus Callosum, which is sometimes challenging to locate[29]. Instead, they proceeded to localize A.C. and P.C. after successfully obtaining the prominent landmark Mid-brain Pons Junction (MPJ) as found from the training dataset. The average Euclidean distance between automatically and manually detected landmarks was found to be 1.1 mm, indicating high accuracy[12].

In the study by Anbazhagan et al., they used non-rigid based registration, adaptive basis algorithm (ABA)[30] to be specific to transform the landmark points from the atlas to the subject space to automate the localization of A.C., P.C., and Mid-sagittal plane. The estimated location of these landmarks is further optimized to achieve a more refined position. This algorithm is evaluated on simulated and real data and has produced promising results. The proposed method offers a time-efficient and reproducible approach to the critical first step of spatial normalization in brain structure[14].

3.4 Chapter Summary

This chapter provides a comprehensive literature survey on detecting anatomical landmarks in brain MRI scans. The survey begins with the work of Xulei Yang et al., who proposed a multi-task deep neural network to simultaneously detect landmarks such as the A.C., P.C., and symmetry lines. This approach improves learning and prediction efficiency by exploiting the similarities and differences across tasks[1]. Another Hiroyuki Sugimori and Masashi Kawakami study proposes the use of a faster region-based convolutional neural network (Faster R-CNN) to detect the orbitomeatal line (OM-line), a standard line for aligning brain MRI scans[19]. Yuan Liu and Benoit Dawant's work focuses on detecting A.C., P.C., and the mid-sagittal plane (MSP) using regression forest models and a hierarchical localization approach[15]. Further, Christine A. Edwards et al. introduce DeepNavNet[20]. This deep learning-based method regresses the 3D coordinates of the A.C. and P.C. Further, we have seen non deep learning-based approaches, like in the work of B. A. Ardekani and A. H. Bachman, presented an automatic model-based approach to detect A.C. and P.C. landmarks on brain MRI scans. Their method, which does not rely on Corpus Callosum localization, achieved a high accuracy of 1.1 mm in landmark detection[12]. In another study, Anbazhagan et al. used non-rigid registration with the adaptive basis algorithm (ABA)[30] to automate the localization of A.C., P.C., and the Mid-sagittal plane. Their approach showed promising results on simulated and real data, offering a time-efficient and reproducible method for spatial normalization in brain structure[14]. This chapter provides an overview of the existing methods and techniques employed for automatic landmark detection in 2D slices and 3D MRI volumes, laying the foundation for the methodology and implementation discussed in later chapters.

CHAPTER 4

Methodology

This chapter details the methodology for A.C. and P.C. localization and Orientation vector prediction. It explains the approach step-by-step, including network architecture and its hyperparameter details, the dataset used, data preprocessing techniques, loss function used, and the specific algorithms or models employed. The rationale behind the selected methodology is thoroughly discussed

4.1 Network Architecture

The deep convolutional neural network (CNN) is a robust and widely used architecture in image data analysis, including classification, regression, and segmentation tasks[31]. In this, we have designed a custom CNN model consisting of three parallel convolution branches, as depicted in Figure 4.1. The CNN model was developed to predict A.C. and P.C. coordinates and orientation vectors in brain MRI images.

To train the model, we used the linear activation function as the output layer for predicting the A.C. and P.C. coordinates, while the sigmoid activation function was employed for angle prediction. The hidden layers of the CNN model utilized the rectified linear unit (ReLU) activation function, which helps introduce non-linearity and capture complex patterns in the data. The detailed specification of the architecture can be seen in the Table 4.1

We have adopted a homogeneous ensemble approach to enhance prediction accuracy and generalization performance. This approach involved training five similar models independently. Five models dedicated to A.C. landmark prediction, another set of five models for P.C. landmark prediction, and an additional five models for angle estimation were individually trained, and output from those five models was subsequently averaged to obtain the final prediction for each respective landmark category, as illustrated in Figure 4.2.

Each model underwent 40 epochs during the training process, with the "Adam" optimizer being utilized. The optimizer is crucial in updating the model's parameters during training to minimize the prediction error. "Adam" is a popular optimization algorithm commonly used in deep learning models due to its effectiveness in handling large-scale datasets and complex architectures. By training the models for multiple epochs, the network had the opportunity to learn intricate patterns and relationships within the data, gradually improving its performance over time.

The ensemble learning approach employed by us provides several benefits. First, it helped mitigate the risk of overfitting, a common challenge in deep learning

models, where the model becomes overly specialized to the training data and performs poorly on unseen examples. By training multiple models independently and combining their predictions, the ensemble model was able to reduce the impact of individual model biases and errors, leading to an improved generalization of unseen data.[32], [33].

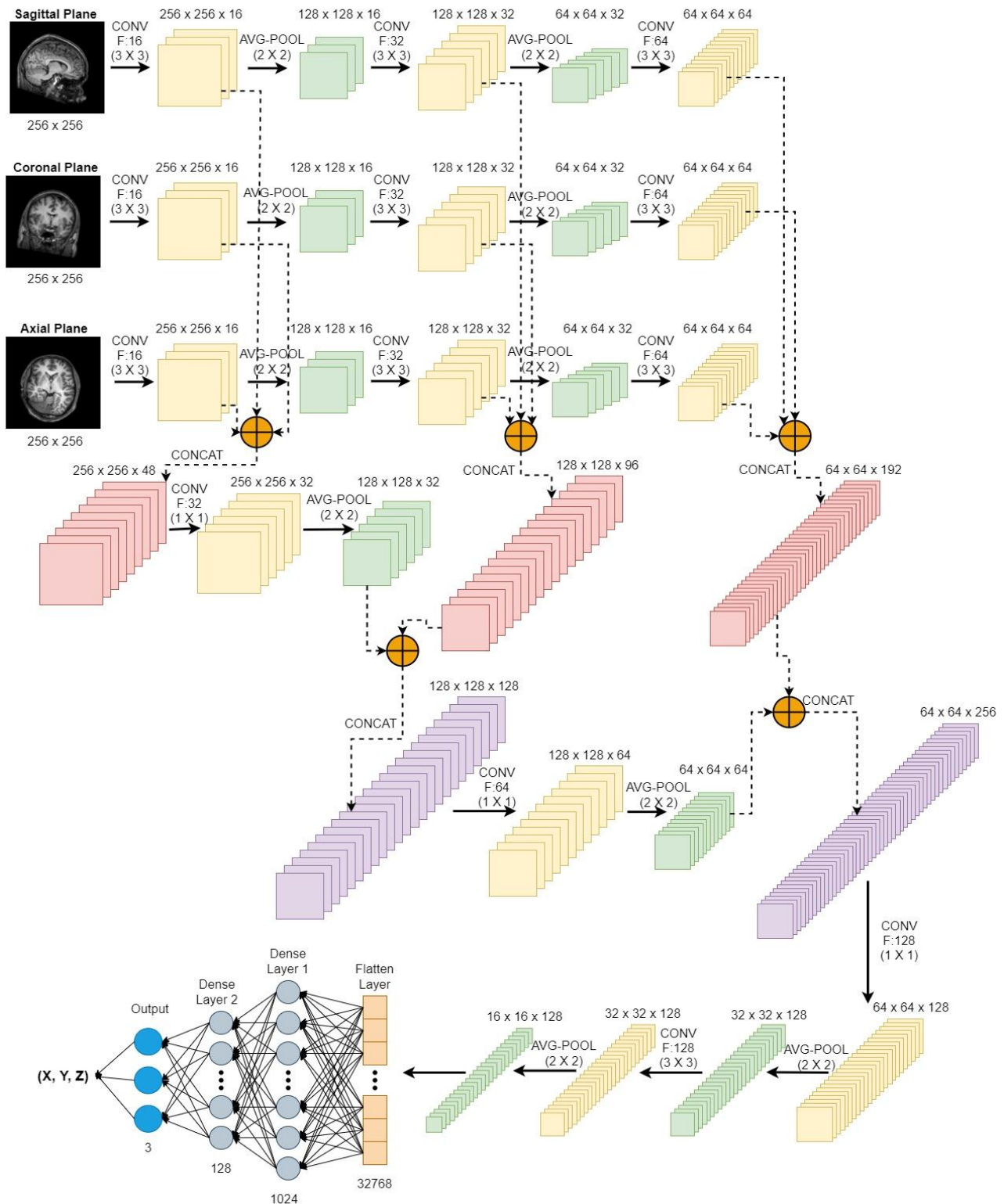


Figure 4.1 Custom CNN architecture

Table 4.1 Architecture Details

Layer	Depth	Filter/Pooling	Output Size	Parameters	Input
input1	1		256 x 256 x 1	0	
input2	1		256 x 256 x 1	0	
input3	1		256 x 256 x 1	0	
conv2d	16	3 x 3	256 x 256 x 16	160	input1
conv2d_1	16	3 x 3	256 x 256 x 16	160	input2
conv2d_2	16	3 x 3	256 x 256 x 16	160	input3
average_pooling2d		2 x 2	128 x 128 x 16	0	conv2d
average_pooling2d_1		2 x 2	128 x 128 x 16	0	conv2d_1
average_pooling2d_2		2 x 2	128 x 128 x 16	0	conv2d_2
concatenate			256 x 256 x 48	0	conv2d, conv2d_1, conv2d_2
conv2d_4	32	3 x 3	128 x 128 x 32	4640	average_pooling2d
conv2d_5	32	3 x 3	128 x 128 x 32	4640	average_pooling2d_1
conv2d_6	32	3 x 3	128 x 128 x 32	4640	average_pooling2d_2
conv2d_3	32	1 x 1	256 x 256 x 32	1568	concatenate
concatenate_1			128 x 128 x 96	0	conv2d_4, conv2d_5, conv2d_6
average_pooling2d_3		2 x 2	128 x 128 x 32	0	conv2d_3
average_pooling2d_4		2 x 2	64 x 64 x 32	0	conv2d_4
average_pooling2d_5		2 x 2	64 x 64 x 32	0	conv2d_5
average_pooling2d_6		2 x 2	64 x 64 x 32	0	conv2d_6
concatenate_2			128 x 128 x 128	0	concatenate_1, average_pooling2d_3
conv2d_8	64	3 x 3	64 x 64 x 64	18496	average_pooling2d_4
conv2d_9	64	3 x 3	64 x 64 x 64	18496	average_pooling2d_5
conv2d_10	64	3 x 3	64 x 64 x 64	18496	average_pooling2d_6
conv2d_7	64	1 x 1	128 x 128 x 64	8256	concatenate_2
concatenate_3			64 x 64 x 192	0	conv2d_8, conv2d_9, conv2d_10
average_pooling2d_7		2 x 2	64 x 64 x 64	0	conv2d_7
concatenate_4			64 x 64 x 256	0	concatenate_3, average_pooling2d_7
conv2d_11	128	1 x 1	64 x 64 x 128	32896	concatenate_4
average_pooling2d_11		2 x 2	32 x 32 x 128	0	conv2d_11
conv2d_12	128	3 x 3	32 x 32 x 128	147584	average_pooling2d_11
average_pooling2d_12		2 x 2	16 x 16 x 128	0	conv2d_12
flatten			32768	0	average_pooling2d_12
dense			1024	33555456	flatten
dense_1			128	131200	dense
dense_2(output)			3	387	dense_1

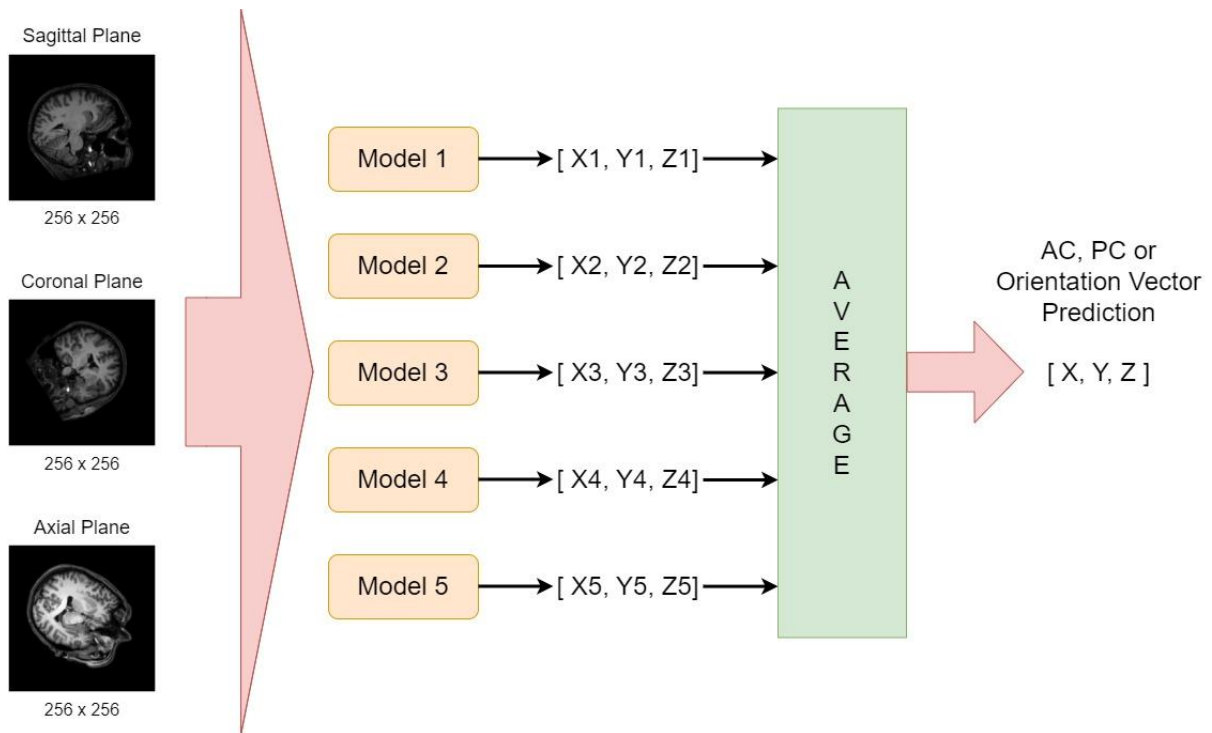


Figure 4.2 Homogeneous Ensemble Model

Three brain MRI localizer slices from the sagittal, coronal, and axial planes were fed into the CNN model for input. These slices provided spatial information for the model to learn and make accurate predictions. The model's output was the 3D coordinates of the A.C. or P.C. landmarks in the brain MRI volume, depending on the task, as well as the orientation vector.

It's important to note that separate models were developed for A.C. and P.C. coordinate prediction and orientation detection, indicating that the network was specialized for each task. This approach allows for better modeling and prediction of the specific anatomical landmarks and angles of interest in the brain MRI data.

4.2 Dataset

In the assessment, a total of six publicly available MRI datasets were utilized (refer to Table 4.2 for details). These datasets were selected based on their relevance to the research objectives and their availability for academic use. The inclusion of multiple datasets allowed for a comprehensive evaluation of the proposed methods and increased the generalizability of the findings. By utilizing these six publicly available MRI datasets and carefully excluding scans with poor data quality, we proceeded with the subsequent stages of data preprocessing, analysis, and interpretation.

Table 4.2 Dataset Details

Dataset	No. of MRI Scan used	Demography	Reference
DS1	35 (36)	Mean Age 20.12, SD : 1.73; 18 females	[34]
DS2	34 (34)	Age: 19 - 35	[35]
DS3	34 (35)	Age:19-31; 21 females	[36]
DS4	30 (36)	Age:18-32, 24 females	[37]
DS5	50 (52)	Age:18-42yrs; 30 females	[38]
DS6	48 (49)	Age:19-29; 24 females	[39]

4.3 Data Pre-processing

In this study, we utilized MRI volumes as the primary data source. Each MRI volume was initially resized to 256x256x256 pixels with an isotropic resolution of 1mm. To enhance the diversity and variability of the dataset, two separate datasets were generated through the application of random affine transformations.

The first dataset was obtained by applying ten random affine transformations with 9 DOF (Degrees of Freedom), including translation, rotation, and scaling. The translations were randomly generated within a range of -20mm to +20mm, rotations ranged from -30° to $+30^\circ$, and a scaling factor of 0.1mm was applied. Consequently, ten MRI brain volumes were generated from a single brain volume, each representing a different transformation.

Further, three-plane MRI localizer slices were extracted from each transformed volume. These slices were obtained by slicing the 3D MRI volume at its center in each of the three axes: sagittal, coronal, and axial planes. As a result, three 2D MRI slices representing the different planes were obtained for each transformed volume. The entire process described above is visually illustrated in Figure 4.3

Similarly, a second dataset was generated using different affine transformations. In this case, the translations ranged from -5mm to +5mm, rotations ranged from -15° to $+15^\circ$, and the scaling factor remained the same at 0.1mm.

By generating these datasets from affine transformation, we aimed to simulate and account for head position and orientation variations commonly encountered in real-world MRI scans. This approach allowed us to train models capable of accurately

predicting the A.C. and P.C. coordinates and the orientation vector, even in the presence of head location inaccuracies

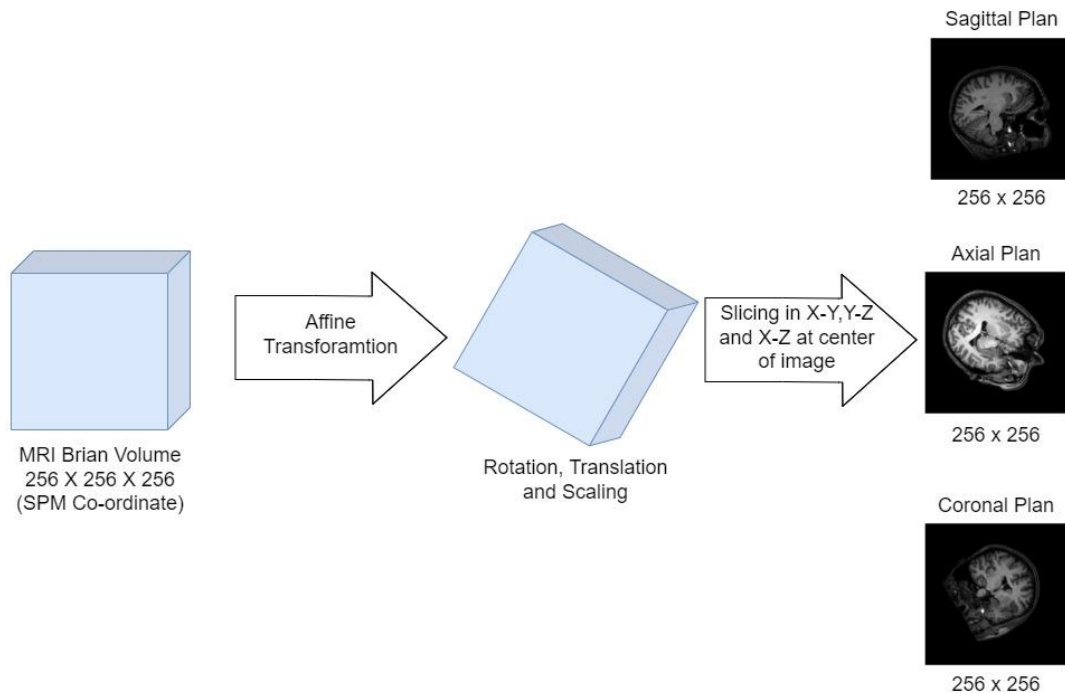


Figure 4.3 Pre-processing of Dataset

4.4 Loss Function

We have used Mean Square Error (MSE) as the loss function for our convolution neural network model. The equation for mean square error is as follows.

$$MSE = \frac{1}{N} \sum_{i=1}^N (y_i - \hat{y})^2$$

Here, “N” represents the total number of test samples used for evaluation. Each sample is denoted by the subscript “i”. The term “ y_i ” corresponds to the ground truth value for the i-th sample, while “ \hat{y} ” represents the predicted output from our CNN model for the same sample.

4.5 Chapter Summary

This chapter discusses the methodology for localizing the A.C. and P.C. landmarks, as well as predicting the orientation vector, in brain MRI scans is presented. The approach involves the development of a custom CNN architecture with three parallel convolution branches, allowing for accurate prediction of A.C. and P.C. coordinates and orientation angles. A homogeneous ensemble model is employed to improve prediction accuracy and generalization, training five similar models independently

and averaging their outputs. The dataset used consists of publicly available MRI datasets, carefully selected to ensure data quality. Data preprocessing techniques include:

- Resizing the MRI volumes.
- Applying random affine transformations to simulate head position variations.
- Extracting three-plane MRI localizer slices.

The mean square error is used as the loss function for training the CNN models. Overall, this comprehensive methodology provides a robust framework for effectively localizing landmarks and predicting orientations in brain MRI scans.

CHAPTER 5

Experiment and Results

The chapter focuses on the practical aspects of implementing the proposed methodology. It describes the experimental setup, model training, testing workflow, evaluation metrics, and the results/outcomes. The results of the experiments, including quantitative performance measures and qualitative analyses, are presented and discussed.

5.1 Training

In our thesis, we adopted a two-stage approach consisting of coarser to finer models. This approach allowed us to progressively refine the accuracy and precision of our predictions. To implement this approach, we trained models on two distinct datasets generated as described in Section 4.2. Further, we have introduced multiple models, which include training and testing our dataset in full resolution, 25%, 5%, and 1% lower-sampled images, each with an ensemble approach, as discussed in Section 4.1.

The first stage involves the training of the coarser model. This model is trained on the dataset with $\pm 20\text{mm}$ translation, $\pm 30^\circ$ rotations, and a scaling factor of 0.1. This allows us to predict the first set of results through which we can adjust and align the patient's head orientation to achieve better and finer results.

The second stage involves training a finer model, which is trained on the dataset with $\pm 5\text{mm}$ translation, $\pm 15^\circ$ rotations, and a scaling factor of 0.1. With this model, we predict the final results for our input image. The detailed workflow for predicting the final image is further explained in the Section 5.3.

We have also performed both within-dataset and cross-dataset evaluations for our model. During the training, 20 MRI scans were randomly selected, each from DS1, DS2, and DS3, and the remaining MRI scans were used for the within-dataset testing. The model was evaluated using MRI scans from DS4, DS5, and DS6 for cross-dataset validation. The Euclidian distance between anatomical landmarks' actual and predicted locations in 3D space was utilized as an error measure.

5.1.1 Low Pass Filtering

In order to obtain the lower-sampled image of the dataset, we employed low-pass filtering in the frequency domain technique. Firstly, we transformed the original dataset into the frequency domain using the Fourier transformation. This transformation allows us to analyze the image in terms of its frequency components.

Next, we applied a low-pass filtering technique to achieve the desired lower-sampled images. This involved creating a mask that defined the frequency range to be preserved while attenuating higher frequencies. The mask was then multiplied with the frequency domain image, effectively reducing the high-frequency details and retaining the lower-frequency components.

Finally, we converted the filtered image back to the spatial domain using the Inverse Fourier transformation. This process restored the image from the frequency domain to its original spatial representation but with a reduced level of detail due to the low-pass filtering.

Applying low-pass filtering means eliminating the high-frequency components from the MRI image in the K-space. The resulting effect is that the Field of View(FOV) of the MRI image remains the same, but the pixel width is increased. Larger the pixel size/width, the lower the in-plane spatial resolution. Hence, to obtain low-resolution images, we have applied low-pass filtering. We have introduced low-pass filtering to mimic the low-resolution MRI images from the MRI scan machine. Further, we can verify whether we can accurately predict A.C., P.C., and orientation vectors in these low-resolution images. Obtaining low-resolution images from the MRI scan machine significantly reduces the MRI acquisition time, reducing overall workflow time.

The Figure 5.1 visually presents the complete process, depicting the conversion from the spatial domain to the frequency domain, the utilization of a low-pass filter, and the subsequent inverse transformation back to the spatial domain.

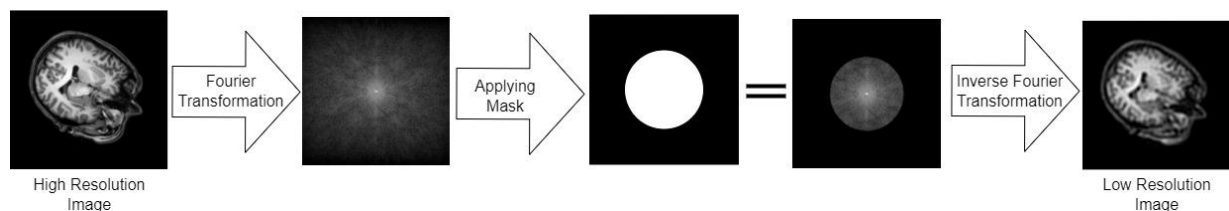


Figure 5.1 Low Pass Filtering using Fourier transformation

The impact of various levels of low-pass filtering can be observed in the accompanying Figure 5.2 - Figure 5.5. Notably, discernible changes can be observed in the images as the filtering intensity increases. The loss of intricate details is attributed to the attenuation of high-frequency components responsible for details, sharpness,

and edge information within the images. As a result, the filtered images exhibit a progressively smoother appearance with diminishing fine information as the level of filtering intensifies. The visual representation of these outcomes effectively demonstrates the effects of Fourier low-pass filtering on the images under consideration.

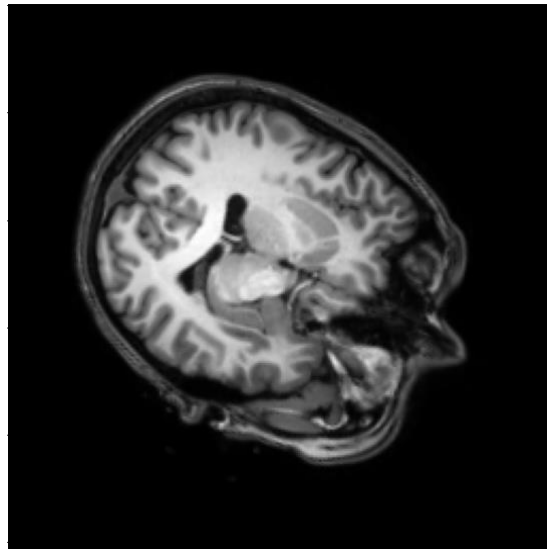


Figure 5.2 Original Image

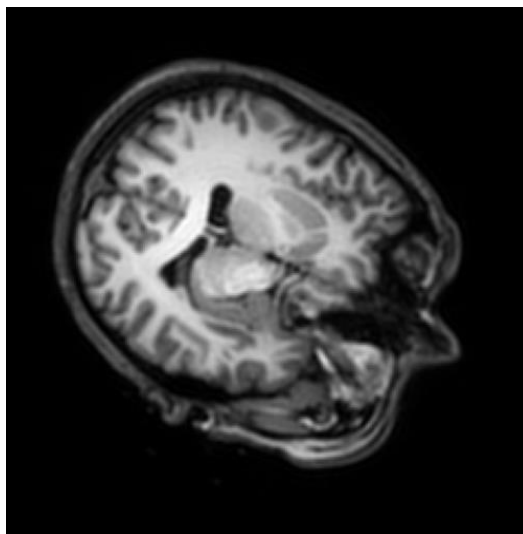


Figure 5.3 25% Low-filtered Image

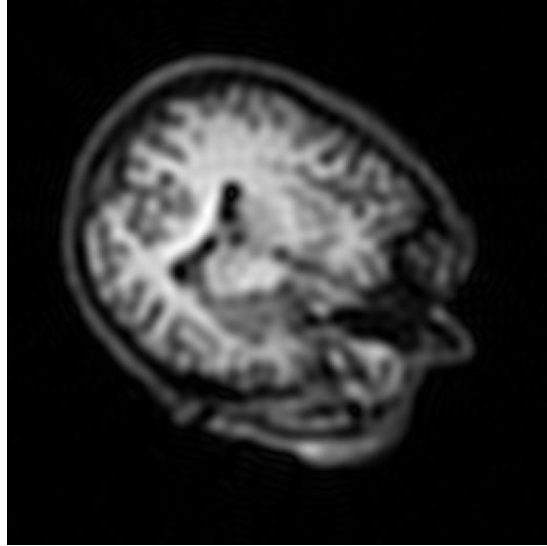


Figure 5.4 5% Low-filtered Image

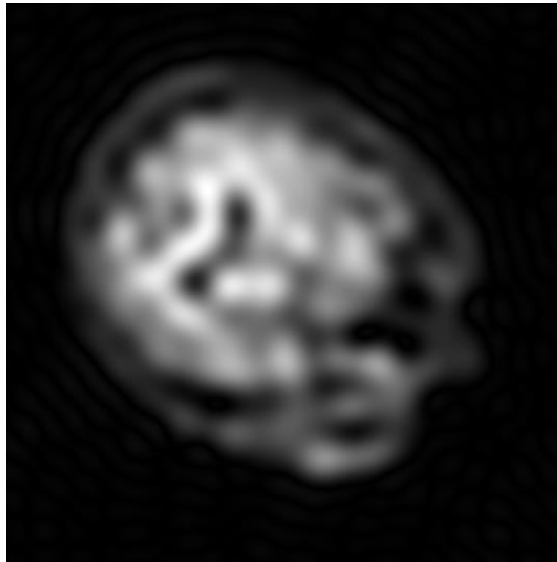


Figure 5.5 1% Low-filtered Image

5.2 Unit Testing

We have done the unit testing of both models. For models trained with $\pm 20\text{mm}$ translation and $\pm 30^\circ$ rotation, the mean A.C. and P.C. landmark localization error is less than 3 millimeters, and the mean error for predicting angle is around 3° for within-dataset across all the models. For cross-dataset, the mean A.C. and P.C. landmark localization error is found to be less than 4 millimeters, and the mean error for predicting angle is around 4° across all the models. (Table 5.1.)

For models trained with $\pm 5\text{mm}$ translation and $\pm 15^\circ$ rotation, the mean A.C. and P.C. landmark localization error is less than 1.5 millimeters, and the mean error for predicting angle is around 1.4° for within-dataset across all the models. For cross-dataset, the mean A.C. and P.C. landmark localization error is found to be less than 2

millimeters, and the mean error for predicting angle is around 1.8° across all the models.(Table 5.2)

Table 5.1 ±20mm Translation and 30°Rotation

	Within Dataset			Cross Dataset		
	A.C.	P.C.	Angle	A.C.	P.C.	Angle
Original	2.64 ± 0.21	2.46 ± 0.33	3.00	3.15 ± 0.31	3.69 ± 0.98	3.88
25% Lower-Sampled	2.68 ± 0.24	2.45 ± 0.27	3.14	3.19 ± 0.37	3.69 ± 1.05	4.00
5% Lower-Sampled	2.67 ± 0.22	2.51 ± 0.35	3.41	3.21 ± 0.39	3.79 ± 1.12	3.98
1% Lower-Sampled	2.73 ± 0.27	2.47 ± 0.29	3.62	3.37 ± 0.41	3.62 ± 1.04	4.17

Table 5.2 ±5mm Translation and 15°Rotation

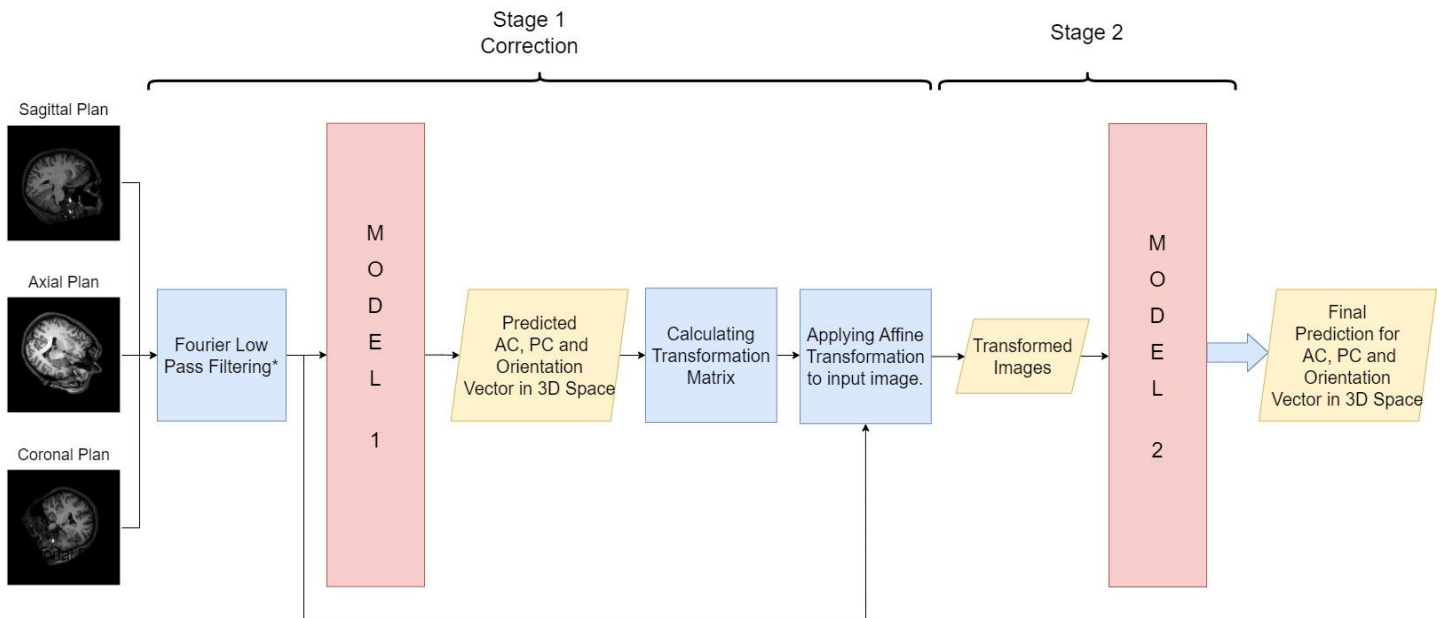
	Within Dataset			Cross Dataset		
	A.C.	P.C.	Angle	A.C.	P.C.	Angle
Original	1.16 ± 0.20	1.44 ± 0.24	1.36	1.47 ± 0.20	1.91 ± 0.40	1.78
25% Lower-Sampled	1.17 ± 0.17	1.45 ± 0.26	1.35	1.44 ± 0.23	1.96 ± 0.35	1.61
5% Lower-Sampled	1.19 ± 0.20	1.42 ± 0.26	1.37	1.47 ± 0.17	1.97 ± 0.42	1.80
1% Lower-Sampled	1.23 ± 0.23	1.43 ± 0.23	1.38	1.52 ± 0.18	1.94 ± 0.34	1.80

5.3 Testing Workflow

Firstly, we obtained three types of image planes - Sagittal, Coronal, and Axial - from datasets containing images with 20mm translation and 30° rotation. These images served as inputs to Model 1. This model has been specifically trained using the dataset that includes images with 20mm translation and 30° rotation. The objective is to use this model to predict the coordinates for the anterior commissure (A.C.), posterior commissure (P.C.), and orientation vector.

Once the predictions for A.C., P.C., and the orientation vector have been obtained, the next step involves calculating the transformation matrices. These matrices enable the application of an affine transformation to the 3D image volume, simulating the necessary correction. Hence, this affine transformation mimics the correction required to align the images accurately.

Following the transformation, three-plane MRI localizer slices are extracted. This is achieved by slicing the 3D MRI volume at the center along each of the three axes, namely the sagittal, coronal, and axial planes. These resulting slices serve as the input for Model 2. Model 2, which has been trained using the dataset comprising images with 5mm translation and 15° rotation, is responsible for predicting the final output based on the provided slices. By employing this two-stage approach, the study aims to refine the predictions and obtain a more accurate estimation of the desired outputs, ultimately contributing to the overall success of the analysis. The complete workflow of the testing can be seen in the Figure 5.6.



* Required only for 25%, 5% and 1% model Testing

Figure 5.6 Testing Pipeline

5.4 Outcomes

Table 5.3 Within Dataset

	A.C. (mean \pm std)		P.C. (mean \pm std)		Angle (mean)	
	Model 1	Model 2	Model 1	Model 2	Model 1	Model 2
Original	1.88 \pm 1.02	0.80 \pm 0.55	1.64 \pm 0.83	0.88 \pm 0.45	3.27	1.35
25% Lower-Sampled	1.76 \pm 0.95	0.79 \pm 0.45	1.62 \pm 0.86	0.95 \pm 0.52	2.81	1.29
5% Lower-Sampled	1.74 \pm 0.89	0.75 \pm 0.38	1.76 \pm 0.74	0.91 \pm 0.47	2.79	1.29
1% Lower-Sampled	1.67 \pm 0.95	0.79 \pm 0.48	1.61 \pm 0.71	0.92 \pm 0.49	2.95	0.79

Table 5.3 shows that the mean error in predicting the A.C. and P.C. is less than 1mm with a standard deviation of less than 0.6mm, while the mean error in predicting the orientation vector is less than 1.4°. Hence, the result produced is as expected with respect to unit testing done on the individual models.

Table 5.4 Cross Dataset

	A.C. (mean \pm std)		P.C. (mean \pm std)		Angle (mean)	
	Model 1	Model 2	Model 1	Model 2	Model 1	Model 2
Original	2.20 \pm 1.10	1.25 \pm 0.66	2.76 \pm 1.67	1.31 \pm 0.72	3.24	1.59
25% Lower-Sampled	2.50 \pm 1.35	1.32 \pm 0.95	2.82 \pm 1.82	1.41 \pm 0.80	3.69	1.78
5% Lower-Sampled	2.49 \pm 1.20	1.30 \pm 0.88	2.96 \pm 1.96	1.41 \pm 0.78	4.27	1.88
1% Lower-Sampled	2.62 \pm 1.31	1.39 \pm 0.91	2.78 \pm 1.78	1.38 \pm 0.73	4.90	1.49

Table 5.4 shows that the mean error in predicting the A.C. and P.C. is less than 1.5mm with a standard deviation of less than 1mm, while the mean error in predicting the orientation vector is less than 2° . Hence, the result produced is as expected with respect to unit testing done on the individual models.

5.5 Chapter Summary

In this chapter, we have evaluated our proposed methodology to predict the A.C. and P.C. landmark localization and determine the orientation vector. This involves training coarser and finer models, which were tested individually. Finally, we have designed the complete testing pipeline, which incorporates the results obtained from the coarser model, calculating the transformation matrix in order to correct the misalignment in the head position and finally giving this input to the finer model to predict the final output. The results are promising and useable in real-world applications.

CHAPTER 6

Discussion and Conclusion

6.1 Discussion

In this study, we have presented a methodology for predicting A.C. and P.C. landmark localization and determining the orientation vector in brain MRI scans. The suggested method entailed developing coarser and finer models that were then evaluated and tested separately. The results demonstrated the effectiveness of our methodology and its potential for real-world applications.

The two-stage training approach, starting with the coarser model and progressing to the finer model, allowed for gradual refinement and improvement in the accuracy and precision of the predictions. This iterative process enabled us to adjust and align the patient's head orientation, leading to more accurate and reliable results.

We also conducted extensive evaluations, including within-dataset and cross-dataset testing, to check the generality and assess our model's performance. The evaluation metrics, such as landmark localization and angle prediction errors, provided quantitative measures of the models' performance. The results from both within-dataset and cross-dataset evaluations showed consistent and favorable outcomes, with low errors in landmark localization and angle prediction.

We have also trained, evaluated, and tested our model with the lower sampled images, which is not yet been researched much. This increases the practical applicability of our solution in the real world as many medical facilities still use MRI machines, which give low-sampled images as output. Another benefit of using low-sampled images is that it takes much less amount of time to acquire them, hence decreasing the overall MRI acquisition time and patient discomfort.

The testing workflow, incorporating the predictions from the coarser model and applying a transformation matrix for head position correction, proved to be a robust and reliable approach. The finer model, trained on images with finer transformations, provided more accurate predictions based on the corrected inputs supplied from the first stage. This two-stage process contributed to the overall success of the analysis and improved the estimation of the desired outputs.

6.2 Conclusion

In conclusion, our study has successfully predicted the A.C. and P.C. landmarks and Orientation vector directly from three-plane 2D MRI Localizer slices. The accuracy in locating these landmarks is comparable to existing methods that predict them in 3D voxel or 2D MRI scans in the mid-sagittal plane. Our methodology demonstrates impressive results, with a mean error of less than 1mm for landmark localization within the dataset and less than 2mm for cross-dataset evaluation. Additionally, the mean error in degrees for determining the orientation vector is less than 2° for both within and cross-dataset analyses. These findings open up possibilities for useful applications like image-guided neurosurgery and neuroimaging research.

6.3 Future Work

The future research includes working directly with the K-space dataset, which encompasses spatial frequency and phase information. This approach could decrease the preprocessing time and computational resources as the output from the MRI scan is in the K-space.

Further, we aim to predict and localize more anatomical landmarks and planes in 3D space, which can aid in treating problem-specific regions, enabling a broader range of applications in neuroimaging research and clinical settings.

Furthermore, we would like to investigate the latest MRI machines and technologies utilized since it is crucial for a comprehensive understanding of the technologies currently employed. For instance, exploring the Achieva 1.5T SE Circular Edition, Siemens MAGNETOM Skyra, and Siemens Numaris XA31 systems can provide insights into their specific capabilities, imaging protocols, and potential optimizations for our methodology. Understanding the intricacies of these MRI machines will help refine our approach and maximize its compatibility and performance within real-world clinical settings.

References

- [1] X. Yang, W. T. Tang, G. Tjio, S. Y. Yeo, and Y. Su, "Automatic detection of anatomical landmarks in brain MR scanning using multi-task deep neural networks," *Neurocomputing*, vol. 396, pp. 514–521, Jul. 2020, doi: 10.1016/j.neucom.2018.10.105.
- [2] B. Gohel, L. Kumar, and D. Shah, "Deep learning-based Automated Localisation of Anterior Commissure and Posterior Commissure Landmarks in 3D space from three-plane 2D MRI localiser slices of the brain," *Procedia Comput. Sci.*, vol. 218, pp. 1027–1032, 2023, doi: 10.1016/j.procs.2023.01.082.
- [3] M. Reuter, E. R. Gerstner, O. Rapalino, T. T. Batchelor, B. Rosen, and B. Fischl, "Impact of MRI head placement on glioma response assessment," *J. Neurooncol.*, 2014, doi: 10.1007/s11060-014-1403-8.
- [4] X. Tao and S. Gupta, "A Method for Correcting Inter-Series motion in Brain MRI for Auto Scan Plane Planning," *Proc. 17th Sci. Meet. Int. Soc. Magn. Reson. Med.*, 2009.
- [5] Y. Li and C. Dumoulin, "Correlation imaging for multiscan MRI with parallel data acquisition.," *Magn. Reson. Med.*, vol. 68, no. 6, pp. 2005–17, Dec. 2012, doi: 10.1002/mrm.24206.
- [6] S. Otake, T. Taoka, M. Maeda, and W. T. C. Yuh, "A guide to identification and selection of axial planes in magnetic resonance imaging of the brain," *Neuroradiology Journal*. 2018. doi: 10.1177/1971400918769911.
- [7] P. K. Mandal, R. Mahajan, and I. D. Dinov, "Structural brain atlases: Design, rationale, and applications in normal and pathological cohorts," *Journal of Alzheimer's Disease*. 2012. doi: 10.3233/JAD-2012-120412.
- [8] K. L. Weiss *et al.*, "Clinical brain MR imaging prescriptions in Talairach space: Technologist- and computer-driven methods," *Am. J. Neuroradiol.*, 2003.
- [9] P. A. Starr, "Placement of deep brain stimulators into the subthalamic nucleus or Globus pallidus internus: technical approach.," *Stereotact. Funct. Neurosurg.*, vol. 79, no. 3–4, pp. 118–45, 2002, doi: 10.1159/000070828.
- [10] D. L. Collins, P. Neelin, T. M. Peters, and A. C. Evans, "Automatic 3D intersubject registration of MR volumetric data in standardized Talairach space.," *J. Comput. Assist. Tomogr.*, vol. 18, no. 2, pp. 192–205, 1994, [Online]. Available: <http://www.ncbi.nlm.nih.gov/pubmed/8126267>
- [11] W. L. Nowinski and A. Thirunavuukarasuu, "Atlas-assisted localization analysis of functional images.," *Med. Image Anal.*, vol. 5, no. 3, pp. 207–20, Sep.

- 2001, doi: 10.1016/s1361-8415(01)00043-3.
- [12] B. A. Ardekani and A. H. Bachman, "Model-based automatic detection of the anterior and posterior commissures on MRI scans," *Neuroimage*, 2009, doi: 10.1016/j.neuroimage.2009.02.030.
- [13] S. Pallavaram *et al.*, "Automated selection of anterior and posterior commissures based on a deformable atlas and its evaluation based on manual selections by neurosurgeons," in *Medical Imaging 2007: Visualization and Image-Guided Procedures*, 2007. doi: 10.1117/12.709936.
- [14] P. Anbazhagan, A. Carass, P. L. Bazin, and J. L. Prince, "Automatic estimation of midsagittal plane and AC-PC alignment based on nonrigid registration," in *2006 3rd IEEE International Symposium on Biomedical Imaging: From Nano to Macro - Proceedings*, 2006. doi: 10.1109/isbi.2006.1625046.
- [15] Y. Liu and B. M. Dawant, "Automatic Localization of the Anterior Commissure, Posterior Commissure, and Midsagittal Plane in MRI Scans using Regression Forests," *IEEE J. Biomed. Heal. Informatics*, 2015, doi: 10.1109/JBHI.2015.2428672.
- [16] P. Rastogi, V. Singh, and M. Yadav, "Deep learning and big datatechnologies in medical image analysis," in *PDGC 2018 - 2018 5th International Conference on Parallel, Distributed and Grid Computing*, 2018. doi: 10.1109/PDGC.2018.8745750.
- [17] P. Rastogi, K. Khanna, and V. Singh, "LeuFeatx: Deep learning-based feature extractor for the diagnosis of acute leukemia from microscopic images of peripheral blood smear," *Comput. Biol. Med.*, 2022, doi: 10.1016/j.compbiomed.2022.105236.
- [18] J. Shi *et al.*, "Applications of deep learning in medical imaging: a survey," *Journal of Image and Graphics*. 2020. doi: 10.11834/jig.200255.
- [19] H. Sugimori and M. Kawakami, "Automatic detection of a standard line for brain magnetic resonance imaging using deep learning," *Appl. Sci.*, 2019, doi: 10.3390/app9183849.
- [20] C. A. Edwards, A. Goyal, A. E. Rusheen, A. Z. Kouzani, and K. H. Lee, "DeepNavNet: Automated Landmark Localization for Neuronavigation," *Front. Neurosci.*, 2021, doi: 10.3389/fnins.2021.670287.
- [21] A. Narayanan *et al.*, "GE Healthcare's AIRx™ Tool Accelerates Magnetic Resonance Imaging using Intel® AI Technologies." [Online]. Available: https://www.intel.com/content/dam/www/public/us/en/ai/documents/AIRx_W_hitepaper_GEHC-Approved.pdf
- [22] F. Renard, S. Guedria, N. De Palma, and N. Vuillerme, "Variability and reproducibility in deep learning for medical image segmentation," *Sci. Rep.*, 2020, doi: 10.1038/s41598-020-69920-0.

- [23] J. Hofmanninger, F. Prayer, J. Pan, S. Röhrich, H. Prosch, and G. Langs, "Automatic lung segmentation in routine imaging is primarily a data diversity problem, not a methodology problem," *Eur. Radiol. Exp.*, 2020, doi: 10.1186/s41747-020-00173-2.
- [24] E. Ntoutsis *et al.*, "Bias in data-driven artificial intelligence systems—An introductory survey," *Wiley Interdiscip. Rev. Data Min. Knowl. Discov.*, 2020, doi: 10.1002/widm.1356.
- [25] A. Baird and B. Schuller, "Considerations for a More Ethical Approach to Data in AI: On Data Representation and Infrastructure," *Frontiers in Big Data*. 2020. doi: 10.3389/fdata.2020.00025.
- [26] D. Caligari Conti, "Magnetic Resonance Imaging," 2016.
- [27] N. B. Smith and A. Webb, *Introduction to Medical Imaging*. Cambridge University Press, 2010. doi: 10.1017/CBO9780511760976.
- [28] R. W. Brown, Y.-C. N. Cheng, E. M. Haacke, M. R. Thompson, and R. Venkatesan, Eds., *Magnetic Resonance Imaging*, 2nd ed. Chichester, UK: John Wiley & Sons Ltd, 2014. doi: 10.1002/9781118633953.
- [29] C. Lee, "Automated segmentation of the corpus callosum in midsagittal brain magnetic resonance images," *Opt. Eng.*, vol. 39, no. 4, p. 924, Apr. 2000, doi: 10.1117/1.602449.
- [30] G. K. Rohde, A. Aldroubi, and B. M. Dawant, "The adaptive bases algorithm for intensity-based nonrigid image registration," *IEEE Trans. Med. Imaging*, vol. 22, no. 11, pp. 1470–1479, Nov. 2003, doi: 10.1109/TMI.2003.819299.
- [31] R. Yamashita, M. Nishio, R. K. G. Do, and K. Togashi, "Convolutional neural networks: an overview and application in radiology," *Insights into Imaging*. 2018. doi: 10.1007/s13244-018-0639-9.
- [32] Y. Ren, L. Zhang, and P. N. Suganthan, "Ensemble Classification and Regression—Recent Developments, Applications and Future Directions [Review Article]," *IEEE Computational Intelligence Magazine*. 2016. doi: 10.1109/MCI.2015.2471235.
- [33] R. S. Akinbo and O. A. Daramola, "Ensemble Machine Learning Algorithms for Prediction and Classification of Medical Images," 2021. doi: 10.5772/intechopen.100602.
- [34] W. Boekel, E. J. Wagenmakers, L. Belay, J. Verhagen, S. Brown, and B. U. Forstmann, "A purely confirmatory replication study of structural brain-behavior correlations," *Cortex*, 2015, doi: 10.1016/j.cortex.2014.11.019.
- [35] W. Boekel, B. U. Forstmann, and M. C. Keuken, "A test-retest reliability analysis of diffusion measures of white matter tracts relevant for cognitive control," in

Psychophysiology, 2017. doi: 10.1111/psyp.12769.

- [36] G. Elliott Wimmer and C. Büchel, "Learning of distant state predictions by the orbitofrontal cortex in humans," *Nat. Commun.*, 2019, doi: 10.1038/s41467-019-10597-z.
- [37] G. E. Wimmer, J. Li, K. J. Gorgolewski, and R. A. Poldrack, "'rewardBeast.'" OpenNeuro, 2021. doi: 10.18112/openneuro.ds002738.v1.0.2.
- [38] O. R. Dobrushina *et al.*, "Modulation of Intrinsic Brain Connectivity by Implicit Electroencephalographic Neurofeedback," *Front. Hum. Neurosci.*, 2020, doi: 10.3389/fnhum.2020.00192.
- [39] S. Jahfari, K. Richard Ridderinkhof, A. G. E. Collins, T. Knäpen, L. J. Waldorp, and M. J. Frank, "Cross-Task Contributions of Frontobasal Ganglia Circuitry in Response Inhibition and Conflict-Induced Slowing," *Cereb. Cortex*, 2019, doi: 10.1093/cercor/bhy076.